Dynamic Stiffness Based Control for a MicroGrid Microsource Interface

Prabath J. Binduhewa, *Member, IEEE*, Mike Barnes, *Senior Member, IEEE*

***Abstract*—Intermittent renewable microsources in so-called MicroGrids will need to have plug-and-play functionality – therefore will need to be integrated with local storage. The design of such cross-coupled non-linear systems is complex and presently focuses on command tracking dynamics. In practice the robustness of such systems to external disturbance inputs plays at least an equal role. This paper presents the dynamic stiffness methodology for such design and illustrates it for a single-phase photovoltaic microsource with battery energy storage. While this method has been applied with considerable success in motor drives (converter plus single load) and UPS systems (converter plus energy storage), it has not so far been applied to the more complex case considered here of a microsource with embedded storage (converter plus energy source plus storage). The mathematical model of the system is derived and presented in state feedback block diagrams whereby local and global external disturbances and cross-coupling are clearly identified. The resulting system is clearly able to prevent the propagation of external disturbances from one end to the other. Experimental results are provided to validate the operation of the proposed controller.**

***Index Terms*— MicroGrid, Microsources, Energy storage, Photovoltaic, Battery storage, Dynamic stiffness**

I. Introduction

ANALYSIS, control and planning of renewable energy generation is a key challenge for future networks. Such generation is intermittent and geographically distributed – in contrast to traditional fossil-fuel based generation. Also in contrast to conventional generation such systems need to be integrated with the utility network at the distribution level [1]. Energy storage is also required to fill gaps between demand and supply.

The concept of a MicroGrid is useful here. This is a small power system which, in theory at least, provides easy integration of renewable energy generation units with variable output [2]-[7]. A typical MicroGrid consists of number of smaller capacity generation units (typically in the range of 100's of Watts to 100's of kW), a local distribution network, local protection system, electrical and heat loads, and a utility network integration unit [2]-[7]. A MicroGrid would typically be integrated to the utility network at a single point, and the advanced internal control of the MicroGrid would be used to prevent internal MicroGrid dynamics from appearing to the utility network [3], [4], [8]-[10]. Such control is complex [11] and no definitive methodology for it has yet been developed. One reason for this is the complexity of potential interactions within the microsource of sub-system dynamics. The resultant combination presents an extremely complex and hard to model system to the distribution network, which would be particularly difficult to handle when multiple microsources are considered. It is thus essential to remove as many of the source sub-system dynamics appearing to the network to reduce the complexity of MicroGrid Control, in essence by decoupling the internal subsystem controllers from the output and making sure each is insensitive to the control behavior of the other subsystems. This paper proposes an approach which does this through a 'Dynamic Stiffness' methodology and so handles this complexity better and is significantly more robust than traditional command tracking only based approaches. This is the first time a dynamic stiffness approach has been applied to microsources with integrated energy storage and the method provides a framework for future research and design. In such systems three sources - the generation, energy storage and grid tied inverter - now vie to control the DC link. Ensuring that the system is 'robust' to the action of each and to external disturbances is thus important but complex. Dynamic stiffness is a highly useful and flexible tool for ensuring this. This application is important because such MicroGrid sources introduce highly distributed energy storage - a relatively new concept - but a very useful one for ensuring security of supply can be maintained despite variability in the renewable generation microsource.

Almost all the microsources within a MicroGrid are connected through an inverter, and the internal energy storage of this inverter is low [3]. Therefore some form of energy storage must be incorporated into the MicroGrid to smooth the fluctuations of renewable microsources to make them appear well-behaved. Storage can be either centralized or distributed

Manuscript received December 2, 2013; revised March 23,2014, June, 1 2014, December, 4, 2014 and February 19,2015; accepted February 23, 2015.

P. J. Binduhewa is with the Department of Electrical and Electronic Engineering, Faculty of Engineering, University of Peradeniya, Peradeniya, Sri Lanka. He was attached to the Power Conversion Group of the University of Manchester, UK. (Corresponding author to provide phone: +94 81 239 3405; fax: +94 81 238 5772; e-mail: prabathb@ee.pdn.ac.lk).

M. Barnes is with The Power Conversion Group, School of Electrical and Electronic Engineering, The University of Manchester, Manchester, UK. (e-mail: mike.barnes@manchesetr.ac.uk).

as presented in Fig. 1 [2], [5]. Distributed storage will enable "plug-and-play" functionality, which states that any microsource should be able to connect at any point without significant changes to the overall structure [3], [4]. This would lead to a smooth, economical and sustainable expansion of MicroGrids. Centralized storage solutions would in contrast require system level upgrades as microsources are added.

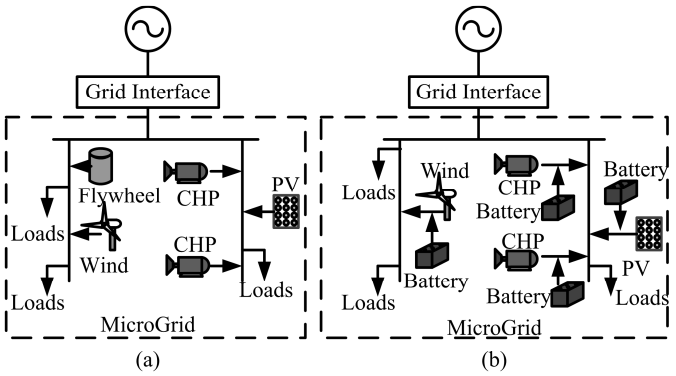

Fig. 1. Storage options for a MicroGrid (a) centralized flywheel storage and (b) distributed battery storage

Integration of storage to the microsource interface ensures that the storage capacity of the MicroGrid is kept sufficient and it also removes the debate over 'who pays for extra storage'. In the CERTS MicroGrid [3], [10],[12]-[13], the battery is directly coupled to the dc-link of the inverter and the disadvantages of the method are (a) little control over charging/discharging current and (b) battery voltage must be equal to the voltage of the dc-link. Other options exist (see section II). Much research has been conducted on three-phase microsource interfaces [10]-[21]. However typically the internal dynamics of the MicroGrid microsource are neglected [22-24] and the focus is solely on the microsource-Microgrid interaction. Sophisticated techniques are then presented to make the microsource robust to disturbances on the MicroGrid side of the connection inverter, but the microsource side is often approximated as a DC source, neglecting dynamics here, which can be complex, especially when a supplementary energy storage unit is included. Furthermore, considering the growth of micro-generation, such as the photovoltaic (PV) industry, there is a significant prospect of more single-phase connections, for example roof-top domestic PV. However here too the focus has been on the interface grid interaction [25], assuming an idealized microsource with negligible dynamics. How to achieve this has not achieved significant attention. Even where sub-system interaction of the aggregate microsource has been considered [26], the focus has typically been only longer time-frames (hours) and the human-machine interface and longer term state-of-charge management.

This paper presents a single-phase Microsource interface with embedded storage via a bi-directional converter. This removes the disadvantages related to direct connection of storage to the dc-link but also the necessary expense of an additional converter. A system which consists of multiple power electronic converters will be a challenge to control due to the presence of external disturbances, such as intermittent power variation in the microsources and MicroGrid transients, and cross-coupled variables. The highly cross-coupled and non-linear system is simplified through state feedback state block diagrams. The key attributes of the material presented in this paper is the dynamic stiffness based controller design [27], [28]. Thereby simple controllers were developed for a complex system and disturbance propagation from one end to another is greatly reduced. In the dynamic stiffness based controller design method, the disturbances acting on the system are analyzed and considered for controller design. The main goal is to minimize the effect of disturbances. The dynamic stiffness approach does this by mapping the 'stiffness' of the system to disturbance inputs against frequency. Dynamic stiffness based controller design is already used in different applications such as electrical drive control, UPS design and industrial automation [27, 28], and an extended overview of the methodology is given in these references. A further issue when multiple microsources are considered is synchronization [20]. This involves supplementary system-wide-control-coordination however and is beyond the scope of this paper.

Section II of this paper presents a literature review on interface solutions. The mathematical model of the proposed system is derived in section III. Dynamic stiffness based controllers for the proposed system is explained in Section IV. Section V provides the experimental results followed by conclusion in Section VII.

II. Proposed Microsource Interface

A typical microsource interface with storage is shown in Fig. 2 [13]. The grid side converter is an inverter. The microsource side converter can be either a dc-dc converter or an ac-dc converter depending on the source.

A MicroGrid may operate in grid-connected mode or autonomous mode, i.e. as a separate power system. Local power source(s), either microsource(s) or storage, are responsible to govern the MicroGrid voltage and frequency in the autonomous mode. All the microsources in CERTS MicroGrid can control the frequency and voltage using the droop-line control technique as shown in Fig. 3(a) [3], [10], [12]-[13]. A master-slave control technique is another way used to control microsources [8], [29]. In this technique, Fig. 3(b), one-microsource is operating under droop control while others operate under active power and reactive power (P-Q) reference control. More than one microsource controls the frequency and voltage in the multi-master slave control technique. This eliminates the instability created by the failure of the master in the master-slave method.

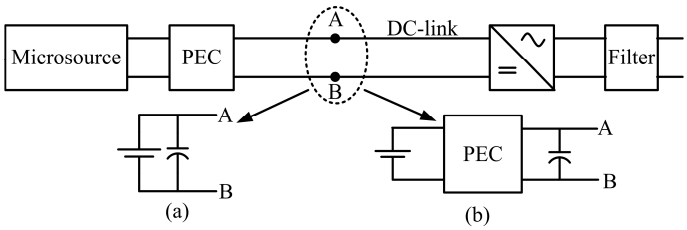

Fig. 2. Typical microsource interface with distributed storage

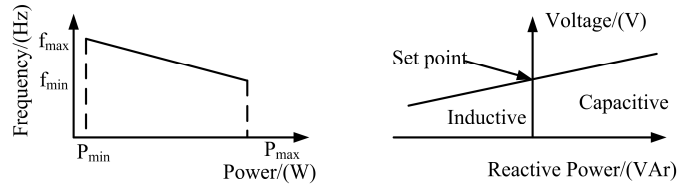

(a) Droop-line controller

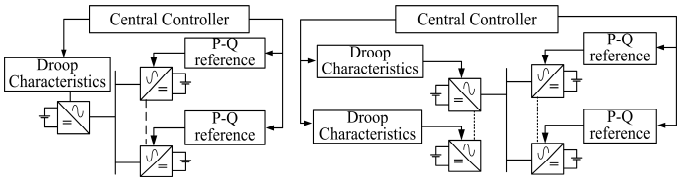

(b) Master-slave and multi-master slave controller

Fig. 3. Microsource controllers

The microsource interface considered in this paper has the structure presented in Fig. 4 which is similar to that in Fig. 2(b). The proposed interface can be divided into two sections based on the functionality. Section-A consists of the microsource and energy storage. Section-B consists of a grid connected single-phase inverter. Power flow control and grid synchronization are the main functions of the single-phase inverter and the inverter sees a stiff dc-link voltage source as the input.

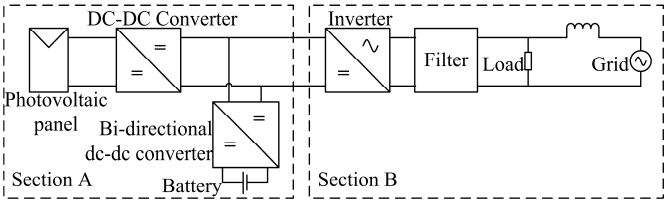

Fig. 4. Proposed microsource interface

The proposed system consists of elements which are subjected to external variations such as microsource output fluctuations with varying environmental conditions, storage capacity and grid voltage. It is important that these disturbances do not interfere with each other or the operation of the systems – the system dynamics should be 'stiff' to such disturbances, though this is frequently inappropriately neglected in system studies. Fundamental to the good functioning of the unit and the interface between section A and B is achieving a dc-link with good disturbance rejection. Here a dynamic stiffness based controller is used to design the controllers in the proposed system, since this allows good frequency domain targeting of the control action and visualization of the problem solution. In order to validate the operation of the system, a photovoltaic panel is considered as the microsource and a lead acid battery bank is considered as the storage.

III. MATHEMATICAL MODEL OF THE PROPOSED SYSTEM

A schematic diagram of the converters used in the proposed system is shown in Fig. 5. A PV panel is connected to the modified forward converter (MFC) [30], [31] which steps up the voltage. The bi-directional dc-dc converter (BDC) couples the battery bank and dc-link [32], [33]. A full-bridge converter is used to convert dc voltage into ac voltage. In order to filter the harmonics, an inductor is coupled in series with the output of the inverter. The transformer provides the electrical isolation.

A. Switch mode converter modeling and linearization

Two operating modes, thus two equivalent circuits, can be found in a typical switch mode dc-dc converter: (a) the on-state and (b) the off-state. The duty ratio, d, of the pulse width modulation (PWM) signal determines operation time of each mode. Equation (1) presents the general representation of the relationship between state variables (x), input (U_i) and disturbances (U_d) of the converter for on-state and off-state. A_1 and A_2 are state matrices, B_1, B_2, D_1 and D_2 are vectors [34]. Equation (2) can be obtained by time weighting and averaging where $d' = (1-d)$ [33]. According (2), it is clear that the system is non-linear as duty ratio and state variable multiplied terms exist.

$$\left.\begin{aligned} \dot{x} &= A_1 x + B_1 U_i + D_1 U_d \quad \text{for } d \cdot T_s \\ \dot{x} &= A_2 x + B_2 U_i + D_2 U_d \quad \text{for } (1-d) \cdot T_s \end{aligned}\right\} \tag{1}$$

$$\begin{aligned} \dot{x} = &\left[A_1 d + (1-d) A_2\right] x + \left[B_1 d + (1-d) B_2\right] U_i \\ &+ \left[D_1 d + (1-d) D_2\right] U_d \end{aligned} \tag{2}$$

The output, y, of a non-linear system is a function of variables x_1 and x_2 according to the Equation (3). The function can be expanded using the Taylor series around the operating point x_{1o} and x_{2o}. Neglecting the higher order terms around the operating point, a linear model in the form of Equation (4) can be obtained. $\Delta y = f(x_1, x_2) - f(x_{1o}, x_{2o})$, $\Delta x_1 = x_1 - x_{10}$ and $\Delta x_2 = x_2 - x_{2o}$, then Equation (5) can be obtained [35].

$$y = f(x_1, x_2) \tag{3}$$

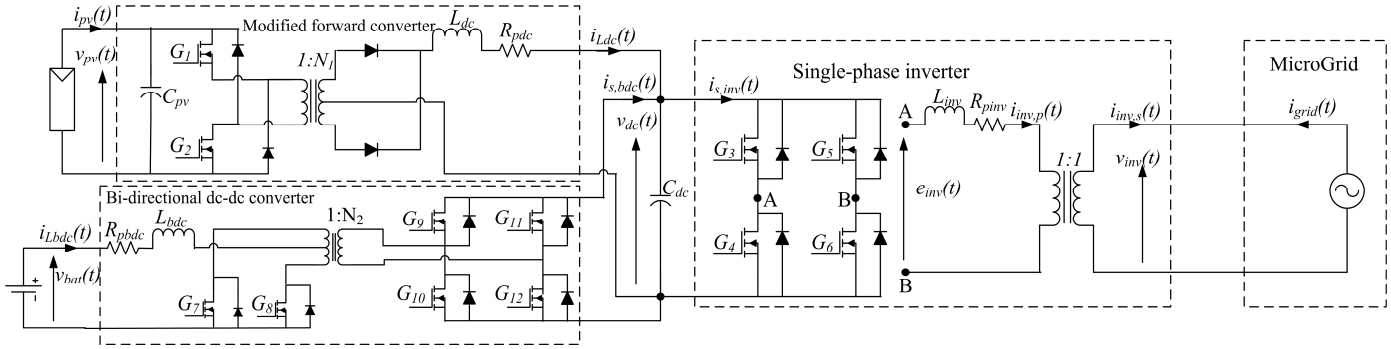

Fig. 5. Schematic diagram of the converters and their controller blocks

$$y \approx f(x_{1o}, x_{2o}) + \frac{\partial f}{\partial x_1}(x_1 - x_{1o}) + \frac{\partial f}{\partial x_2}(x_2 - x_{2o}) \quad (4)$$

$$\Delta y \approx \left.\frac{\partial f}{\partial x_1}\right|_{x_1=x_{10},x_2=x_{20}} \Delta x_1 + \left.\frac{\partial f}{\partial x_2}\right|_{x_1=x_{10},x_2=x_{20}} \Delta x_2 \quad (5)$$

Using this linear approximation, equation (2) can be expressed as in equation (6) where $A = A_1 D_o + (1 - D_o)A_2$, $B = B_1 D_o + (1 - D_o)B_2$ and $D = D_1 D_o + (1 - D_o)D_2$, and operating point values are represent with subscript 'o'. The higher order terms links to the detailed sudden changes to the system. This system contains a number of capacitive and inductive elements, thus the voltage at various points and current flowing through various paths will be relatively slower and smaller. The controller is not expected to deal with very sudden changes – indeed these are typically dealt through protection system. Thus it is reasonable to neglect the higher order terms in this case.

$$\Delta\dot{x} = A\Delta x + B\Delta u_i + D\Delta u_d + \left[(A_1 - A_2)x_o + (B_1 - B_2)u_{i,o} + (D_1 - D_2)u_{d,o}\right]\Delta d \quad (6)$$

B. Mathematical model of the proposed system

The MFC and BDC are switch-mode converters. The on-state and off-state equivalent circuits of the MFC were obtained and presented in the form of (1). Using the state equations of the modes, the average state equations were obtained in the form of (2). The linearized model of the MFC is presented in (7) which was obtained using (1) to (6). The operating point model of the BDC was obtained in the same way and Equation (8) describes the operating point model. The output current of the MFC is given by (9) and the output current of BDC is given by (10). Duty ratio of MFC and BDC are represented by Ddc and Dbdc respectively.

$$i_{odc}(t) = i_{s,inv}(t) - i_{s,bdc}(t) \quad (9)$$

$$i_{obdc}(t) = i_{s,inv}(t) - i_{Ldc}(t) \quad (10)$$

A full-bridge inverter is used and is controlled using a PWM signal. The output filter determines the dynamics of the inverter assuming the dynamics of the inverter are very fast. Thus the governing equation of the inverter is represented in (11). The controller signal, $v_c(t)$ is related to the $e_{inv}(t)$ according to (12).

$$e_{inv}(t) = v_c(t).v_{dc}(t) \quad (12)$$

Table I presents the variable to be controlled, cross-coupled state variable and external disturbance acting on each converter.

IV. State Feedback Block Diagram Reduction and Dynamic Stiffness for Controller Design

A. State feedback block diagram reduction

According to Table I, it is clear that the proposed microsource interface is highly cross-coupled system after linearization. State feedback state block diagrams (SFSB) of the converters and the proposed controllers are presented in Fig. 6. A number of techniques can be used to make the problem tractable.

The MFC has to control the input voltage of the converter. Both input current and inductor current can be lumped together and considered as a disturbance for input voltage control to simplify the SFSB here. The controller of the BDC consists of two loops. The inner loop controls the battery current and the outer loop controls dc-link voltage. In the case of the inner loop, battery voltage and dc-link voltage are coupled together and can be considered as the disturbance. Here it is assumed that the inner loop is faster than the outer loop, thus cascaded control design can be used.

TABLE I
CROSS-COUPLED VARIABLES AND DISTURBANCES

Converter	Output	Cross-coupled	Disturbance
MFC	Input voltage (V_{pv})	Inductor current (I_{Ldc})	Input current (I_{pv})
BDC	Battery current (I_{Lbdc})	DC-link voltage (V_{dc})	-
	DC-link voltage (V_{dc})	Duty ratio	BDC output current (I_{obdc})
Inverter	Inverter current ($I_{inv,p}$)	DC-link voltage (V_{dc})	Grid voltage (V_{inv})

$$\begin{bmatrix}\Delta\dot{v}_{pv}(t)\\ \Delta\dot{i}_{Ldc}(t)\\ \Delta\dot{v}_{dc}(t)\end{bmatrix} = \begin{bmatrix}0 & -\frac{N_1 D_{dco}}{C_{pv}} & 0\\ \frac{N_1 D_{dco}}{L_{dc}} & \frac{R_{pdc}}{L_{dc}} & -1\\ 0 & -\frac{N_1 D_{dco}}{C_{dc}} & 0\end{bmatrix}\begin{bmatrix}\Delta v_{pv}(t)\\ \Delta i_{Ldc}(t)\\ \Delta v_{dc}(t)\end{bmatrix} + \begin{bmatrix}-\frac{N_1 I_{Ldco}}{C_{pv}}\\ \frac{N_1 V_{pvo}}{L_{dc}}\\ 0\end{bmatrix}\left[\Delta d_{dc}(t)\right] + \begin{bmatrix}\frac{1}{C_{pv}} & 0\\ 0 & 0\\ 0 & -\frac{1}{C_{dc}}\end{bmatrix}\begin{bmatrix}\Delta i_{pv}(t)\\ \Delta i_{odc}(t)\end{bmatrix} \quad (7)$$

$$\begin{bmatrix}\Delta\dot{i}_{Lbdc}(t)\\ \Delta\dot{v}_{dc}(t)\end{bmatrix} = \begin{bmatrix}-\frac{R_{pbdc}}{L_{bdc}} & \frac{D'_{bdco}}{N_2 L_{bdc}}\\ -\frac{D'_{bdco}}{N_2 C_{dc}} & 0\end{bmatrix}\begin{bmatrix}\Delta i_{Lbdc}(t)\\ \Delta v_{dc}(t)\end{bmatrix} + \begin{bmatrix}-\frac{1}{L_{bdc}} & \frac{V_{dco}}{N_2 L_{bdc}}\\ 0 & \frac{-I_{Lbdco}}{N_2 C_{dc}}\end{bmatrix}\begin{bmatrix}\Delta v_{bat}(t)\\ \Delta d'_{bdc}(t)\end{bmatrix} + \begin{bmatrix}0 & \frac{1}{C_{dcv}}\end{bmatrix}\left[\Delta i_{obdc}(t)\right] \quad (8)$$

$$\left[\dot{i}_{inv,p}(t)\right] = \left[-\frac{R_{pinv}}{L_{inv}}\right]\left[i_{inv,p}(t)\right] + \left[\frac{1}{L_{inv}}\right]\left[e_{inv}(t)\right] + \left[-\frac{1}{L_{inv}}\right]\left[v_{inv}(t)\right] \quad (11)$$

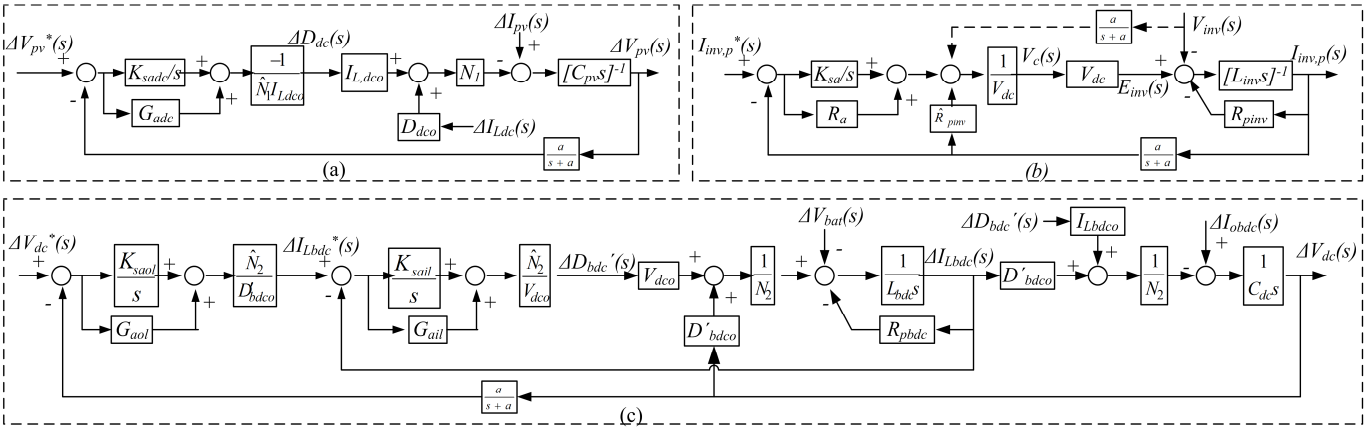

Fig. 6. Controller block diagrams of converters (a) modified forward converter, (b) single-phase inverter, and (c) bi-directional dc-dc converter

The effect of dc-link voltage can be removed inside the controller of inverter if the dc-link voltage is made a feedforward measurement. Also the state feedback of inductor current through internal resistance is decoupled inside the controller. Since the state feedback block diagram is a graphical representation of the state equations, the cross-coupling variables and disturbances can be identified easily. This enables well-defined controllers to be developed while removing cross coupling variables.

B. Dynamic stiffness based controller design for the proposed system

The output of a physical system can be represented as in (13) where *Y*, *X* and *D* are output, input and disturbance [36]. In classical control techniques the effect of disturbance is neglected and only command tracking is considered when designing controllers. This is the approach taken by prior MicroGrid microsource designers. This neglects the critical factor destabilizing a physical system which is the disturbances. In this paper dynamic stiffness properties are utilized for the controller design. Dynamic stiffness (DS) can be defined as disturbance per unit output – see (14) [27], [28]. Indirectly dynamic stiffness provides information on disturbance rejection (DR) ability of the system. In addition the controller can be tuned based on the frequency response of the disturbance.

Dynamic stiffness of the current controller of the inverter, input voltage controller of the MFC, inner current controller of the BDC and outer voltage controller of the BDC are given in (15) to (18) respectively.

$$Y(s)=\left.\frac{Y(s)}{X(s)}\right|_{D(s)=0}X(s)+\left.\frac{Y(s)}{D(s)}\right|_{X(s)=0}D(s) \tag{13}$$

$$DS=\frac{1}{DR}=\frac{D(s)}{Y(s)} \tag{14}$$

$$\frac{V_{inv}(s)}{I_{inv}(s)}=-\left(L_{inv}s+\frac{aR_as+aK_{sa}}{s(s+a)}\right) \tag{15}$$

$$\frac{\Delta I_D(s)}{\Delta V_{in}(s)}=C_{pv}s+\frac{a}{s}\left(\frac{G_{adc}s+K_{sadc}}{s+a}\right) \tag{16}$$

$$\frac{\Delta V_D(s)}{\Delta I_{ind}(s)}=L_{bdc}s+R_{Pbdc}+G_{ail}+\frac{K_{sail}}{s} \tag{17}$$

$$\frac{\Delta I_D(s)}{\Delta V_{DC}(s)}=C_{dc}s+\frac{a(G_{aol}s+K_{saol})}{s(s+a)} \tag{18}$$

In case of inverter, disturbance input decoupling will further improve the dynamic stiffness of the system. It is assumed that parameter estimation and decoupling are ideal. It is clear that in all the controllers high frequency dynamic stiffness is governed by the internal storage element of in the converter. The low-frequency dynamic stiffness depends on the controller parameters.

V. Design and Implementation of a Prototype of Proposed System

A prototype was implemented to evaluate the proposed microsource interface and the controllers, and Table II summarizes the specification of the prototype system. The proposed system was modeled in EMTDC/PSCAD software and implemented in hardware. A photovoltaic emulator was used as the microsource for hardware testing [37]. The SM110-24P PV panel was considered, which delivers 110 W at 35 V during standard test conditions [38]. Lead acid batteries were taken as the storage medium. Four 12 V batteries were connected in series to form the storage. For this analysis, a fraction of open-circuit voltage method is used as the maximum power point tracking method for the PV panel.

TABLE II
Specifications of the Implemented System

Parameter	Value
Power rating of the system	200 W
Rated DC-link voltage, V_{DC}	360 V
MicroGrid voltage, V_{INV}	230 V
Rated battery voltage, V_{bat}	48 V
Switching frequency MFC, f_{MFC}	40 kHz
Switching frequency BDC, f_{BDC}	20 kHz
Switching frequency of inverter, f_{INV}	15 kHz
Turns ratio of transformer in MFD, $1{:}N_1$	1:26
Turns ratio of transformer in BDC, $1{:}N_2$	1:6
DC-link capacitance, C_{dc}	1970 µF
Inductance, L_{dc}	14.9 mH
Inductance, L_{bdc}	0.303 mH
Inductance, L_{inv}	54.8 mH
Capacitance, C_{pv}	3300 µF

A. Dynamic stiffness analysis of the controllers

The dynamic stiffness of the current controller for the inverter was examined for different PI controller gains as given in Table III. Figs. 7 and 8 show the dynamic stiffness and command tracking response around the operating frequency of the current controller. Dynamic stiffness properties are better as the gains are increased. At this point we now can consider command tracking. Command tracking error with respect to ideal (unity gain, 0dB case) decreases with gain parameter increase. As the gains are increased, phase error too increases. The low frequency command tracking can be approximated to (19) which shows the reason for the leading phase angle and above issue. Thus gains for case III were selected for this application as a good compromise between good response (Fig. 8 and Table III) and good disturbance rejection (Fig. 7 and Table III). Overall system performance is better than if only command tracking had been used.

$$\frac{\Delta I_{INV,P}(s)}{\Delta I_{INV,P}^{*}(s)} \approx \frac{(aR_a + K_{sa})s + aK_{sa}}{aR_a s + aK_{sa}} \tag{19}$$

Similarly the controllers for the MFC and BDC were developed using dynamic stiffness analysis. Fig. 9 and 10 present the dynamic stiffness plot of the controllers associated with MFC and BDC. Table IV summarizes the gains and locations of eigenvalues of the dc-dc converters.

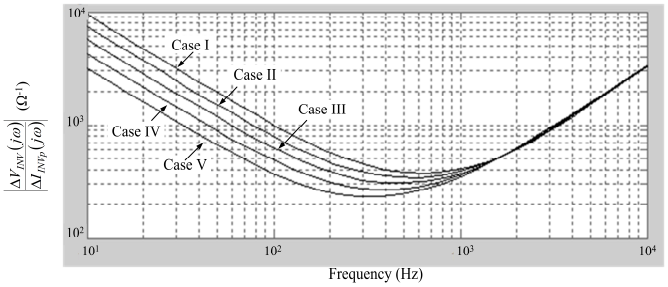

Fig. 7. Dynamic stiffness of the current controller of the inverter

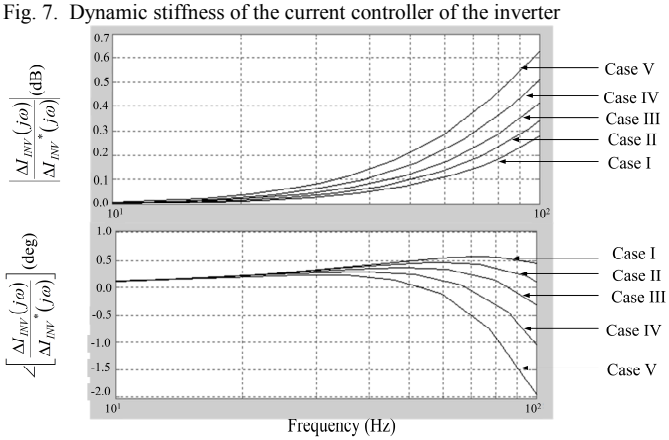

Fig. 8. Command tracking response of the inverter around 50 Hz

TABLE III
CONTROLLER GAINS AND EIGENVALUES

	R_a	K_{sa}	Eigenvalues
Case I	400	$6.00\text{x}10^5$	3200, 1300, 322
Case II	360	$4.65\text{x}10^5$	3450, 1000, 273
Case III	320	$3.60\text{x}10^5$	3660, 929, 236
Case IV	280	$2.70\text{x}10^5$	3840, 779, 201
Case V	240	$2.00\text{x}10^5$	4000, 635, 175

TABLE IV
CONTROLLER GAINS AND EIGENVALUES

dc-dc Converter	Loop	Gains		Eigenvalues
Modified forward (MFC)	Inner loop	G_{adc}	0.25	4.82 kHz, 8.62 Hz,
		K_{sadc}	3.00	2.45 Hz
Bi-directional dc-dc (BDC)	Inner loop	G_{ail}	0.75	471 Hz, 133 Hz
		K_{sail}	750	
	Outer loop	G_{aol}	0.01	64.8 Hz, 16.9 Hz
		K_{saol}	0.03	

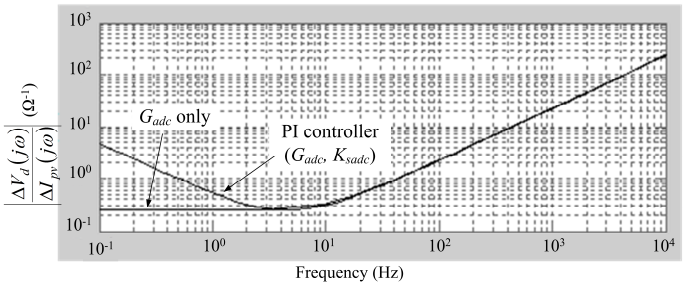

Fig. 9. Dynamic stiffness plot of MFC dc-dc converter

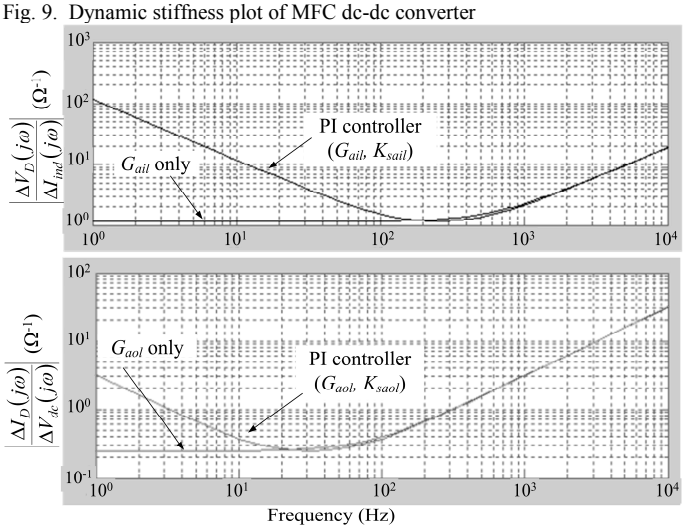

Fig. 10. Dynamic stiffness plot of bi-directional dc-dc converter (inner loop at the top and the outer loop at the bottom).

For all the controllers high frequency dynamic stiffness is determined by the local storage element of the converter. The low frequency dynamic stiffness can be adjusted from PI controller gains. The integral gain is responsible for the very low frequency disturbances and it enables to achieve infinite dynamic stiffness at zero frequency. The dynamic stiffness plots clearly indicate the effect of gains of a PI controller on suppressing disturbances. Also the frequencies which are affected more can be identified. In a particular system, disturbances may occur in a certain frequency ranges and according to this method controller gains can be selected in such a way that dynamic stiffness is higher in those ranges. In this application the selection of gains for the inverter is an example.

B. Behavior of the system under different conditions

Fig. 11 presents the image of the microsource interface implemented in hardware. In order to evaluate the performance of section-A, it was tested in isolation feeding a resistive load. Fig. 12 presents response of the system to a sudden loss of

microsource power. The PV panel voltage settles to an open-circuit voltage – see Fig. 12 (bottom curve). In response, the battery starts to discharge. This is indicated by the positive current in the middle plot. The dc-link voltage drops due to loss of PV output but as the battery starts to discharge, the dc-link voltage is restored back to its rated value. Experimental performance results indicate that linear approximation of the system was reasonable.

The response of the system for a sudden loss of load is presented in Fig. 13. According to the top graph, the dc-link experiences an increase in voltage due the disconnection of load but within one second, voltage is restored to the reference. In response the battery charging current has increased as indicated in middle graph. However minimal variation is visible in the voltage of the PV panel.

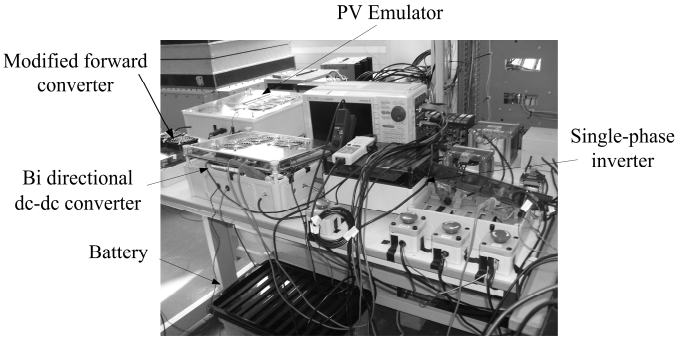

Fig. 11. Experimental set-up of the proposed interface

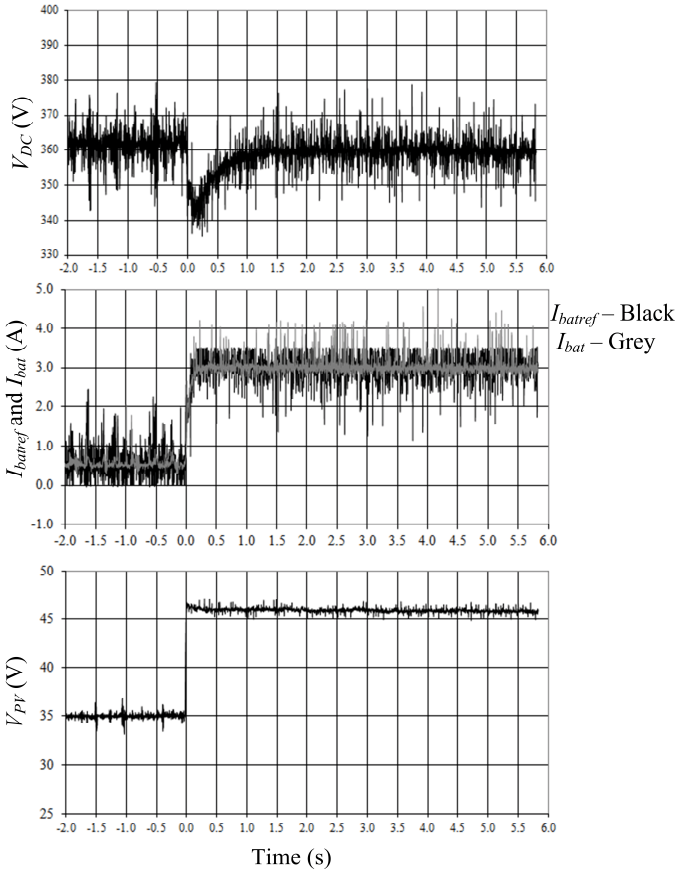

Fig. 12. Behavior of the section-A to sudden microsource output disconnection – experimental results

Therefore notably the disturbance in the load has not propagated to the microsource. Section-A has been successfully designed to track commands but also be robust to disturbances.

The magnitude and phase of the current reference can be calculated from the active and reactive power references according to (20) and (21). Active and reactive power references are noted by P_{ref} and Q_{ref}. $V_{INV,rms}$ is the rms voltage of the load. $I_{INV,ref,mag}$ and $I_{INV,ref,phase}$ are magnitude and phase of the current reference.

$$I_{INV,ref,mag} = \frac{\sqrt{2\left(P_{ref}^2 + Q_{ref}^2\right)}}{V_{INV,rms}} \tag{20}$$

$$I_{INV,ref,phase} = \tan^{-1}\left(\frac{P_{ref}}{Q_{ref}}\right) \tag{21}$$

The response of the current controller at steady state supplying 100 W active power and zero reactive power is shown in Fig. 14. The top graph shows the reference current and the measured current fed to the current controller. The controller follows the current command. The middle graph indicates that the output the three inputs to the decoupling node is dominated by the inverter output voltage – the disturbance. In this case, additionally disturbance decoupling reduces the workload of the controller. The controller output, which is to be fed to the pulse width modulator, is sinusoidal.

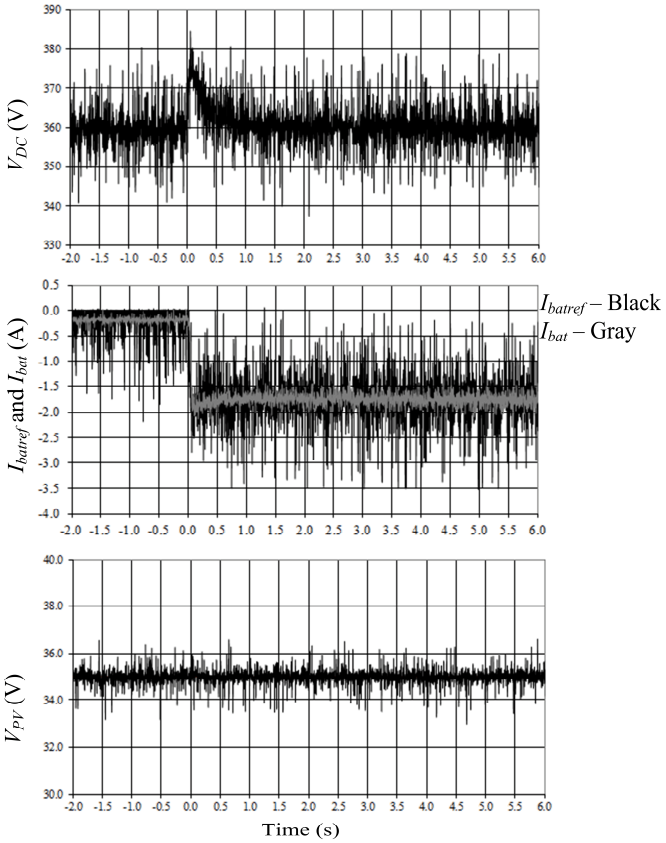

Fig. 13. Behavior of the section-A to sudden load disconnection - Experimental results

The inverter was synchronized to the MicroGrid and the active power reference was ramped to 100 W while the reactive power reference was set to zero. The top plot of Fig. 15 shows that the inverter output current is gradually increased. The MicroGrid current supplied to the local reduces as a result – bottom plot of Fig. 15.

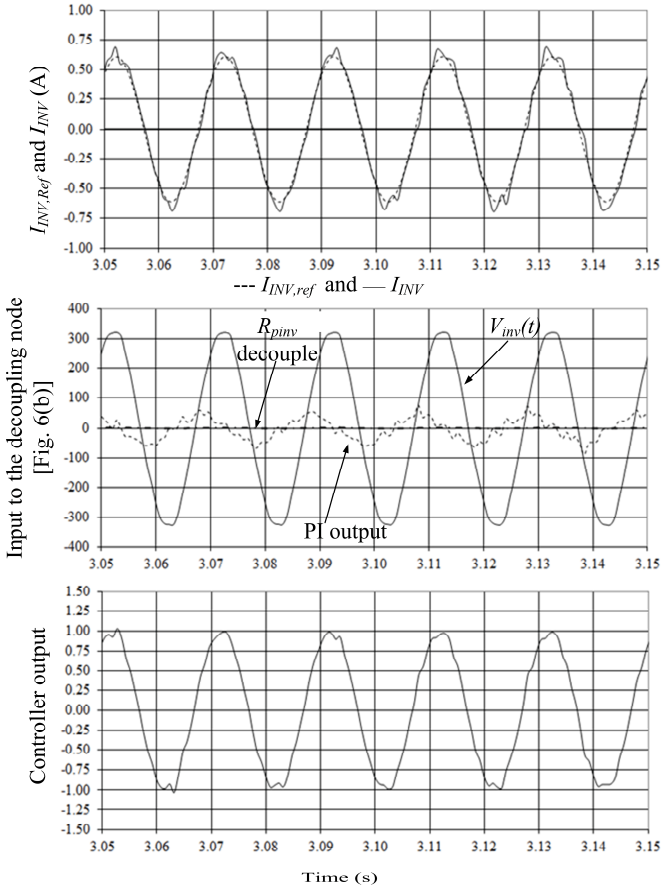

Fig. 14. Behavior of the current controller of the inverter – Experimental results

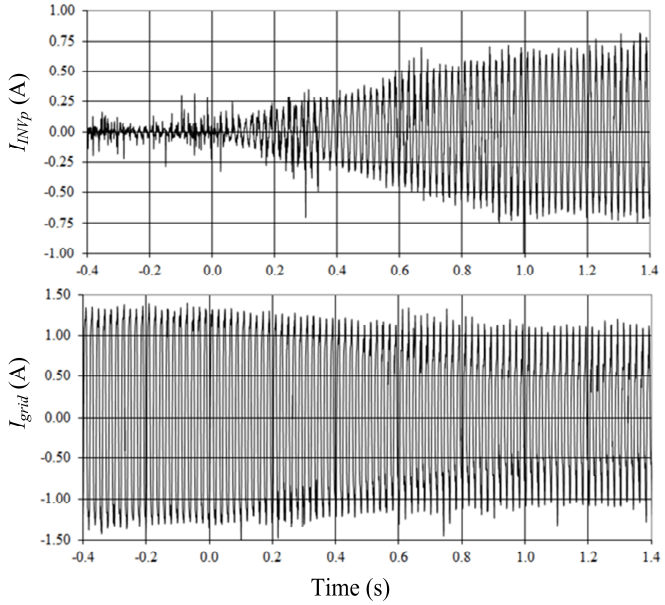

Fig. 15. Experimental inverter output current and grid current

Reference and calculated (based on measurements) active power during grid connection are shown in Fig. 16.The phase error is zero between the inverter output voltage and current verifying that no reactive power is delivered (Fig. 17. top curve). The output with a reactive power reference at 60 VAr is presented in Fig. 17 (bottom curve). According to (20), the phase difference should be 31º and the measured phase difference matches with the calculations.

VI. Conclusion

A single-phase microsource interface with embedded storage was proposed in this paper to achieve a better plug-and-play functionality than a microsource alone. This system is a solution to allow the storage capacity in a MicroGrid to be adjusted dynamically to the proper level as more microsources are added.

Microsource interfaces based on renewable energy sources and embedded with storage are highly complex. This paper presents a framework to analyze such a complex system with multiple disturbances acting on it and having cross-coupled variables. The gains selected clearly indicated the relationship to disturbances with the aid of dynamic stiffness plots. This is beneficial in controller design.

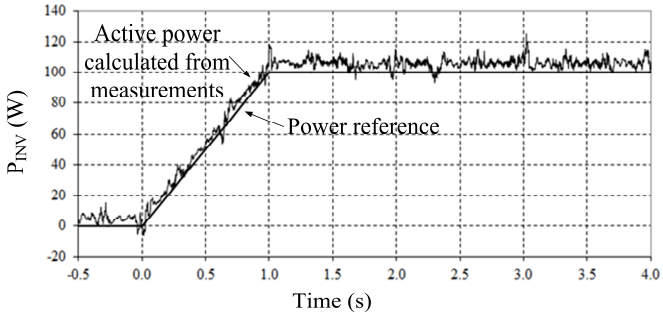

Fig. 16. Active reference to the controller and calculated active power based on the experimental measurements

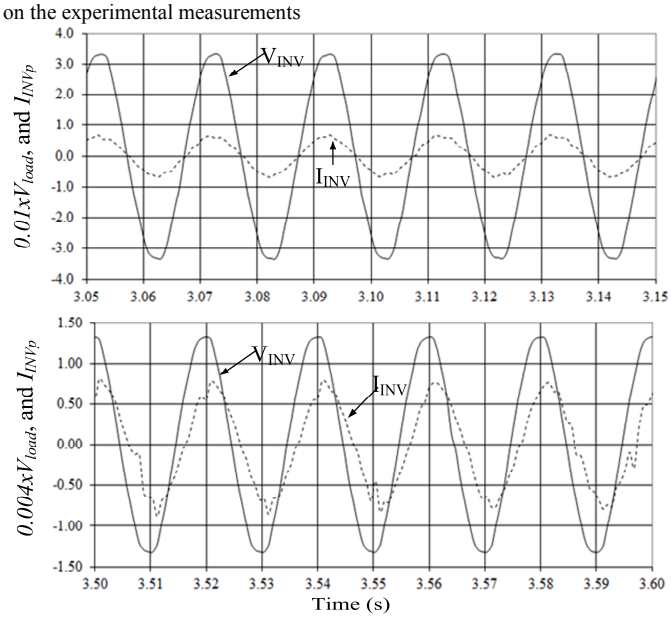

Fig. 17. Experimental inverter output voltage (scaled) and current: Top graph – when reactive power reference is zero, Bottom graph – when reactive power reference is 60 VAr

The designed controller was robust and showed very little disturbance cross-coupling. Therefore this method is particularly applicable to a MicroGrid system with a number of local generators and loads which dynamically vary with time and if there is limited prior knowledge about the system.

This paper's contribution is two-fold: firstly it shows the viability of a small-scale microsource embedded energy storage – such systems have either been separate units or much larger three-phase systems. The paper shows that such systems can be designed to be robust and respond well to external and internal disturbances and changes. Secondly it shows to how to integrate the different sub-units into a coherent and robust system. The methodology used is the dynamic stiffness methodology which is new in the field of MicroGrids, though has been used to good effect in the fields of drives and UPS systems. However there the converter and another single unit were integrated; here the converter and multiple units are integrated. This is important since the microsource, storage and inverter might otherwise complete to control the DC link, significantly disrupting the control of the other units. The research shown in this paper thus provides a framework for the design of such microsource system as well as other multi-stage units.

ACKNOWLEDGMENT

Authors would acknowledge the EPSRC for providing necessary funding for the project through EPSRC UK-MicroGrid project (EP/C00177X/1) and Prof. R. D. Lorenz of the University of Wisconsin-Madison for his helpful discussions during the research.

REFERENCES

[1] Antonis G. Tsikalakis, and Nikos D. Hatziargyriou, "Centralized Control for Optimizing Microgrids Operation," *IEEE Trans. Energy Convers.*, Vol. 23, No. 1, pp. 241-248, Mar. 2008

[2] M. Barnes, J. Kondoh, H. Asano, J. Oyarzabal, G. Ventakaramanan, R. Lasseter, N. Hatziargyriou, and T. Green, "Real-World MicroGrids - An Overview," *proc. IEEE Systems Engineering conf.,* pp. 1-8, 2007

[3] R.H. Lasseter, "MicroGrids," *Proc. IEEE Power Engineering Society Winter Meeting*, Vol. 1, pp. 305-308, 2002

[4] Lasseter, R.H., "Smart Distribution: Coupled Microgrids," *Proc. IEEE*, Vol. 99, No. 6, pp. 1074-1082, June 2011

[5] N. Hatziargyriou, H. Asano, R. Iravani, and C.A.M.C. Marnay, "Microgrids," *IEEE Power Energy Mag.*, Vol. 5, No. 4, pp. 78-94, July/Aug. 2007

[6] Kanchev, H.; Di Lu; Colas, F.; Lazarov, V.; Francois, B., "Energy Management and Operational Planning of a Microgrid With a PV-Based Active Generator for Smart Grid Applications," *IEEE Trans. Ind. Electron.,* Vol. 58, No. 10, pp. 4583-4592, Oct. 2011

[7] Kumar Nunna, H.S.V.S.; Doolla, S., "Multiagent-Based Distributed-Energy-Resource Management for Intelligent Microgrids," *IEEE Trans. Ind. Electron.,* Vol. 60, No. 4, pp. 1678-1687, April 2013

[8] H. Al-Nasseri, M.A. Redfern, and R. O'Gorman, "Protecting micro-grid systems containing solid-state converter generation," *Proc. Int. Conf. Future Power Systems,* p. 5 pp., Nov. 2005

[9] N. Jayawarna, C. Jones, M. Barnes, and N. Jenkins, "Operating MicroGrid Energy Storage Control during Network Faults," *Proc. IEEE Systems Engineering conf.,* pp. 1-7, 2007

[10] H. Nikkhajoei and R.H. Lasseter, "Microgrid Protection," *Proc. IEEE Power Engineering Society General Meeting*, pp. 1-6, 2007

[11] Tenti, P.; Costabeber, Alessandro; Mattavelli, P.; Trombetti, D., "Distribution Loss Minimization by Token Ring Control of Power Electronic Interfaces in Residential Microgrids," *IEEE Trans. Ind. Electron.,* Vol. 59, No. 10, pp. 3817-3826, Oct. 2012

[12] Lasseter, R.H.; Eto, J.H.; Schenkman, B.; Stevens, J.; Vollkommer, H.; Klapp, D.; Linton, E.; Hurtado, H.; Roy, J., "CERTS Microgrid Laboratory Test Bed," *IEEE Trans. Power Del.,* Vol. 26, No.1, pp. 325,332, Jan. 2011

[13] G. Venkataramanan and M. Illindala, "Microgrids and sensitive loads," *Proc. Power Engineering Society Winter Meeting*, Vol.1, pp. 315-322, 2002

[14] M. Barnes, A. Dimeas, A. Engler, C. Fitzer, N. Hatziargyriou, C. Jones, S. Papathanassiou, and M. Vandenbergh, "MicroGrid Laboratory Facilities," in *Proc. Future Power Systems conf.*, pp. 1-6, 2005

[15] N. Pogaku, M. Prodanovic, and T.C. Green, "Modeling, Analysis and Testing of Autonomous Operation of an Inverter-Based Microgrid," *IEEE Trans. Power Electron.*, Vol. 22, pp. 613-625, 2007

[16] Jinwei He; Yun Wei Li, "Generalized Closed-Loop Control Schemes with Embedded Virtual Impedances for Voltage Source Converters with LC or LCL Filters," *IEEE Trans. Power Electron.,* Vol. 27, No. 4, pp. 1850-1861, April 2012

[17] M. Prodanovic and T.C. Green, "High-Quality Power Generation Through Distributed Control of a Power Park Microgrid," *IEEE Trans. Ind. Electron.*, Vol. 53, No. 5, pp. 1471-1482, Oct. 2006

[18] S. Dasgupta, S. N. Mohan, S. K. Sahoo and S. K. Panda, "Lyapunov Function-Based Current Controller to Control Active and Reactive Power Flow From a Renewable Energy Source to a Generalized Three-Phase Microgrid System," *IEEE Trans. Ind. Electron.*, Vol. 60, No. 2, pp. 799 – 813, Feb. 2013

[19] J.A.P. Lopes, C.L. Moreira, and A.G. Madureira, "Defining control strategies for MicroGrids islanded operation," *IEEE Trans. Power Syst.*, Vol. 21, No. 2, pp. 916-924, May 2006

[20] Vasquez, J.C.; Guerrero, J.M.; Savaghebi, M.; Eloy-Garcia, J.; Teodorescu, R., "Modeling, Analysis, and Design of Stationary-Reference-Frame Droop-Controlled Parallel Three-Phase Voltage Source Inverters," *IEEE Trans. Ind. Electron.,* Vol. 60, No. 4, pp. 1271-1280, April 2013

[21] F. Katiraei, R. Iravani, N. Hatziargyriou, A. Dimeas, "Microgrids management", *IEEE Power Energy Mag.*, Vol. 6 , Issue. 3, pp. 54 – 65, 2008

[22] A. Kahrobaeian and Y. A. I. Mohamed, "Suppression of Interaction Dynamics in DG Converter-Based Microgrids Via Robust System-Oriented Control Approach," *IEEE Trans. Smart Grid*, Vol. 3, No. 4, pp. 1800-11, Dec. 2012

[23] Chia-Tse Lee, Chia-Chi Chu and Po-Tai Cheng, "A New Droop Control Method for the Autonomous Operation of Distributed Energy Resource Interface Converters", *IEEE Trans. Power Electron.*, Vol. 28, No. 4, pp. 1980-1993, April 2013

[24] Mehdi Savaghebi, Alireza Jalilian, Juan C. Vasquez, and Josep M. Guerrero, "Autonomous Voltage Unbalance Compensation in an Islanded Droop-Controlled Microgrid," IEEE *Trans. Ind. Electron.*, Vol. 60, No. 4, pp. 1390-1402, April 2013

[25] Jinwei He, Yun Wei Li, and Frede Blaabjerg, "Flexible Microgrid Power Quality Enhancement Using Adaptive Hybrid Voltage and Current Controller," *IEEE Trans. Ind. Electron.*, Vol. 61, No. 6, pp. 2784-2794, June 2014

[26] Manuela Sechilariu, Baochao Wang, and Fabrice Locment, "Building Integrated Photovoltaic System With Energy Storage and Smart Grid Communication," *IEEE Trans. Ind. Electron.*, Vol. 60, No. 4, pp. 1607-1618, April 2013

[27] P. B. Schmidt and R. D. Lorenz, "Design principles and implementation of acceleration feedback to improve performance of DC drives," *IEEE Trans. Ind. Appl.*, Vol. 28 , No. 3, pp. 594 – 599, May/June 1992

[28] Michael J. Ryan, William E. Brumsickle, and Robert D. Lorenz, "Control Topology Options for Single-Phase UPS Inverters," *IEEE Trans. Ind. Appl.*, Vol. 33, No. 2, pp. 493-501, Mar/Apr. 1997

[29] J.A. Pecas Lopes, C.L. Moreira, A.G. Madureira, F.O. Resende, X. Wu, N. Jayawarna, Y. Zhang, N. Jenkins, F. Kanellos, and N. Hatziargyriou, "Control Strategies for MicroGrids Emergency Operation," *Proc. Int. Conf. Future Power Systems*, pp. 1-6, 2005

[30] K. Billngs, "Switchmode Power Supply Handbook", 2nd ed., McGraw-Hill, Chapter 10, pp. 2.80-2.83, 1999

[31] A. I. Pressman, K. Billings, T. Morey, "Switching Power Supply Design", 3rd ed., McGraw-Hill, Chapter 2, pp. 94-98, 2009

[32] T. Mishima and E. Hiraki, "A dual voltage power system by battery/supercapacitors hybrid configuration", *Proc. IEEE 36th Power Electronics Specialist Conf. (PESC)*, pp. 1845-1850, 2005

[33] M. Cacciato, F. Caricchi, F. Giuhli, E. Santini, "A critical evaluation and design of b-directional DC/DC converters for super-capacitors interfacing in fuel cell applicatons", *Proc. IEEE 39th IAS Ann. Meeting, Industry Application Conf.*, Vol. 2, pp. 1127-1133, 2004

[34] Ned Mohan, Tore M. Undeland, and William P. Robbins, *Power Electronics – Converters, Applications and Design*, 3rd ed., John Wiley & Sons, Inc;, pp. 301-353, 2003

[35] Katsuhiko Ogata, *Modern Control Engineering*, 4th ed., Prentice-Hall of India, pp. 112-114, 2002

[36] Robert W. Erickson, and Dragan Makimovic, *Fundamentals of Power Electronics,* 2nd ed., Kluwer Academic Publishers Group, pp. 265-330, 2004

[37] P. J. Binduhewa, and M. Barnes, "Photovoltaic Emulator", *Proc. IEEE 8th Int. Conf. Industrial and Information System*., pp. 519-524, 2013

[38] "Shell SM110-24P photovoltaic solar module datasheet," *http://www.powerupco.com/panels/shell/Shell%20SM110-24P.pdf last accessed on 2010.02.24*.

Prabath J. Binduhewa (M'12) is born in Sri Lanka. He graduated from University of Peradeniya, Sri Lanka in 2005 as an Electrical and Electronic Engineer. He earned his PhD from University of Manchester, UK in 2010.

He is presently attached to the Department of Electrical and Electronic Engineering, University of Peradeniya, Sri Lanka as Senior lecturer. His research interests include MicroGrids, DC Grids, photovoltaic system and power electronics.

Mike Barnes (M'96–SM'07) received the B.Eng. and Ph.D. degrees from the University of Warwick, Coventry, U.K.

In 1997, he was appointed as a lecturer with the University of Manchester Institute of Science and Technology (UMIST, now merged with The University of Manchester), Manchester, U.K., where he is currently Professor of Power Electronic Systems. His research interests cover the field of power-electronics-embedded power systems, advanced drives, VSC-HVDC and FACTS.